

Characterizations of AMPF Micro-Crystals for Photonic, Dielectric, Nano-Influx and Anti-diabetic Relevances

R. HARIHARASUTHAN^a, K.S. RADHA^b,
M. MEENA^c AND K. SENTHILKANNAN^{d,*}

^aDepartment of Chemistry, S.A. Engineering College, Poonamalle, Chennai-600 077, Tamilnadu, India

^bDepartment of Chemistry, R.M.D Engineering College, Chennai-601 206, Tamilnadu, India

^cDepartment of Chemistry, R.M.K Engineering College, Chennai-601 206, Tamilnadu, India

^dDepartment of Physics, Saveetha School of Engineering, SIMATS, Thandalam, Chennai-602 105, Tamilnadu, India

Received: 12.11.2022 & Accepted: 26.01.2023

Doi: [10.12693/APhysPolA.143.309](https://doi.org/10.12693/APhysPolA.143.309)

*e-mail: mcsgoldmedalist@yahoo.in

The bulk AMPF crystals (i.e., 2-amino 4-methyl pyridinium fumarate crystals) are grown by the methodology of slow evaporation; the identified crystalline parameters are 5.0234, 20.0146, 10.8852 — all in units of Å, and $\beta = 95.767^\circ$. The macro-crystals are finely grounded and effectively milled to microscaling-crystals, which has been well confirmed by the morphological pattern by scanning electron microscope studies. The dielectrics of the μ -AMPF crystals are evaluated by the effect on dielectric constant and loss factors as well as AC conductivity and activation energy. The results promptly and adequately identified the suitability of μ -AMPF as a semi-conducting material and its processing in the production of electro-optical devices. The absorbance, photonic, and fluorescence studies on μ -AMPF reveal (i) cut-off value of 260 nm and 290–1100 nm range representing near-zero absorbance and projected for non-linear optical material applications; (ii) band gap of 4.77 eV obtained by Tauc's plot; (iii) value 390 nm obtained with the violet fluorescence emission. The negative type of photoconductivity is observed for μ -AMPF and the non-linearity seen in the absorbance study is the cause for phase matching utility with 121 mV value for a referenced significance of 55 mV. The nano-influx for AMPF is 4.9989 micrometers. The α -glucosidase anti-diabetic activity for versatile scales is also reported.

topics: μ -dielectrics, μ -electronics, μ -photonics, nano-influx

1. Introduction

Our main aim is to grow microscaling-AMPF-type of crystals for photonic, electronic, influx, and biological utilities. Organic crystal sample has a predominance in its behaviour over its counter-parting materials in terms of non-linearity and other sorts of applications and dependencies in computational ways and also experimental modes. μ -AMPF is a versatile kind of organic specimen as it is created by the projected and milled impact of bulk-scaled AMPF. It has profound applications in the pharmaceutical and electric/electronic sectors because of the presence of pyridine and fumaric acid in the entitled specimen. Due to the sort of electrons in the crystal, μ -AMPF has enhanced non-linear optic (NLO) and phase matching, but also particulate of transparency nature as observed in the absorbance and the specific impacts in the value of band-gap in the μ -AMPF crystalline sample.

The literature reports that 2-amino-4-methylpyridinium 4-hydroxybenzoate was grown in 2016, 2-amino-4-methylpyridinium 4-methoxybenzoate dehydrate was grown in 2017, whereas in 2016 2-amino-4-methylpyridinium 2-(4-nitrophenyl)acetate was grown. All of these above-mentioned are the basis for the growth of AMPF micro-scale crystal.

Based on proper equipment, μ -AMPF is studied for single crystal XRD; dielectrics; UV-visible and fluorescence (FL) spectra; Tauc's plot; electronic study by LM 317 controlling of voltage and nano-influx. Photoconductivity and phase matching impact are inferred and reported with other results.

The development of electronic, photonic and display devices is based on current knowledge or is driven by utility outcomes. Here our AMPF is designated for microscaling-photonic-type devices and for use in electronic micro-scaled sectors based on interferences.

From futuristic perspective, the sample can be employed for μ -AMPF-based anti-diabetic, anti-cancer, anti-oxidant drugs. The futuristic perspective can be extended to the production of burglar alarms and switching devices with significantly prolonged activity, possible to be used in a pharmaceutical way.

2. Synthesis

AMPF bulk crystal is synthesized when colourless small needle-like crystals are harvested during a growth period of 16–18 days. Then, one properly incorporates fumaric acid as well 2-amino 4-methylpyridium in the customary 1:1 mode with the solvent as water. Next, all is further milled for 24–48 h uniformly to obtain a miniature of the bulk crystal known as μ -AMPF crystals.

3. Characterizations

3.1. XRD

The XRD data represents the monoclinic crystal system with grouping $P2_1/n$. The crystal parameters a , b , c are 5.0234, 20.0146, 10.8852, respectively, all in units of Å; β is 95.767° . The AMPF empirical formula is $C_{10}H_{12}N_2O_4$.

3.2. AMPF micro-crystal dielectric studies

The dielectric studies illustrate the effects of frequency and temperature in micro-structured materials on the conduction phenomenon. The electrical properties of grain boundaries can be effectively studied by dielectric behaviour. The electrical processes and different polarisation mechanisms that have taken place in the synthesized AMPF micro-crystals have been verified by the analysis of dielectric parameters, namely dielectric loss ($\tan(\delta)$), dielectric constant (ϵ_r), and AC conductivity (σ_{AC}) as a function of frequencies starting from 50 Hz to 5 MHz at various temperatures (313–373 K). The prepared materials are pelleted by using hydraulic pressure and the silver paste is coated on both sides of the pellet to increase the conductivity. The dielectric constant calculated as a function of frequency at various temperatures in the range 313–373 K with an interval of 10 K is depicted in Fig. 1. For all those temperatures, the dielectric constant has a higher value in the low-frequency region (<50 Hz), then decreases with the applied high frequency (5 MHz), and therefore the dielectric constant it has been found to decrease with an increased frequency. In nature, the real part of the dielectric constant (ϵ_r) tends to be extremely dispersive for all the above temperatures below 1 kHz frequency. This dielectric irregularity is caused by polarization of the space charge [1].

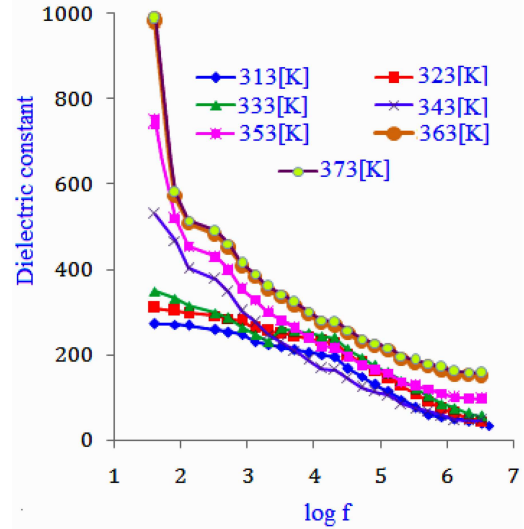


Fig. 1. Variation of dielectric constant with log frequency at different temperatures for synthesized AMPF micro-crystal.

Space charge polarization effect becomes marginal at higher frequencies because the dielectric dispersion is controlled at higher frequencies primarily by intrinsic mechanisms of dielectric polarisation [1–3]. According to Koops et al. [4], weak conducting grain boundaries play a vital role at low frequencies, whereas grain conduction plays a dominant role at higher frequencies. The electrons hop ions by conducting grains and accumulate at the less conducting grain boundaries at lower frequencies, thus inducing polarization of space charge [3, 4]. This is also the cause of high values of dielectric constant (ϵ_r) at low frequencies in the current study. Maxwell et al. [5] and Koops et al. [4] have also reported that the induced dipole moments do not synchronise with the alternating electric field at higher frequencies, which reduces the likelihood of finding electrons at the grain boundary [5]. Due to this reason, the present analysis of synthesised AMPF micro-crystals shows a small constant value of the dielectric constant at larger frequencies.

Figure 2 shows the variation of the dielectric loss with respect to the logarithm of frequency at various temperatures 313, 323, 333, 343, 353, 363, and 373 K. In Fig. 2, it is found that the loss angle ($\tan(\delta)$) also displays similar frequency variation at different temperatures as for the dielectric constant. It is already known that a reduction in grain size increases the sum of grain boundaries and as a result, dielectric loss and dielectric constant decrease. These materials will be suitable for high-frequency applications [6]. In Figs. 3 and 4, respectively, the dielectric constant (ϵ_r) and dielectric loss ($\tan(\delta)$) are plotted as a function of temperature at various frequencies 100 Hz, 1, 10, 100 kHz, and 1 MHz to distinguish the effect of intrinsic dielectric

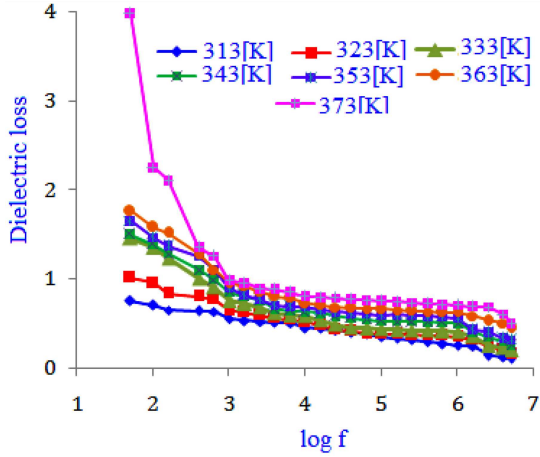


Fig. 2. Variation of dielectric loss with log frequency at different temperatures for synthesized AMPF micro-crystal.

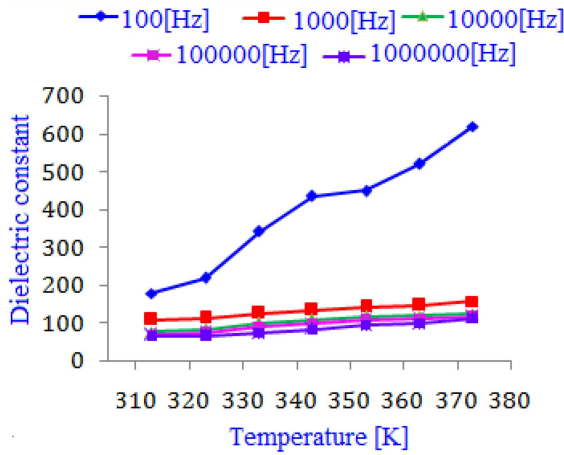


Fig. 3. Temperature dependence of dielectric constant for synthesized AMPF micro-crystal.

polarisation. The polarisation of space charge with variations is properly specified for kilo Hz and Hz. It can be seen in Fig. 3 that the values of the dielectric constant increase with an increase in temperature for all defined frequencies. This dielectric behaviour makes the synthesized AMPF micro-crystals a suitable semiconductor material [7].

The variation of dielectric constant with the temperature at various frequencies can be described as follows. Initially, with increasing temperature, there is a slight increase in the dielectric constant, because the low-temperature thermal energy is not sufficient to free up the localized electric dipoles. These dipoles seek to reorient themselves in the direction of the externally applied electric field. As the temperature increases, more localized dipoles are produced and aligned in the alternating field applied. This causes the dielectric constant (ϵ_r) to increase sharply to reach a maximum value at a temperature called the transition temperature,

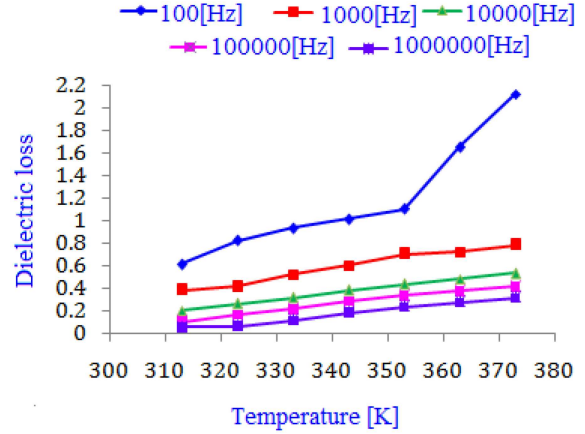


Fig. 4. Temperature dependence of dielectric loss for synthesized AMPF micro-crystal.

which is beyond our instrument detection limit [8]. In the current study, the rate of increase of the dielectric constant with respect to temperature is substantially greater for lesser frequencies (below ~ 10 kHz), while for higher frequencies (100 kHz, 1 MHz) the dielectric constant is considerably low. This peculiar pattern of variation of dielectric constant with temperature at low and higher frequencies can be interpreted as follows: space charge, dipolar, ionic and electronic states are the main polarization states correlated with the dielectric constant [9]. At low frequency, all processes lead to overall polarizability and hence, the dielectric constant is maximum at low frequency. In Fig. 3, it is clearly seen that the dielectric constant measured at 1 kHz, 10 kHz, 100 kHz, and 1 MHz shows a gradual rise up to 343 K and then increases swiftly. This pattern is also seen for other frequencies. Space charge and dipolar polarization are strongly influenced by temperature and play a key role at low frequencies. Hopping of charge carriers is enabled by the rise in temperature [10]. Interfacial polarization increases with temperature at low frequencies because of the increased accumulation of charges along grain boundaries. Dipolar polarization is due to the orientation of dipoles in the presence of an external electric field. Due to the increase in entropy, the arrangement of dipoles becomes difficult with increasing temperature so the dipolar polarization decreases with temperature. Based on the above interpretation, it is understood that the overall increase in dielectric constant with temperature implies that the space charge polarisation is prevailing over the dipolar polarisation in the current study. The ionic and electronic polarisation states primarily contribute to the dielectric constant at higher frequencies. Since these states are almost temperature independent, the dielectric constant at high temperatures and frequencies reaches low and stagnant values [9, 10]. The low value of dielectric loss at high frequency shows that the synthesized AMPF

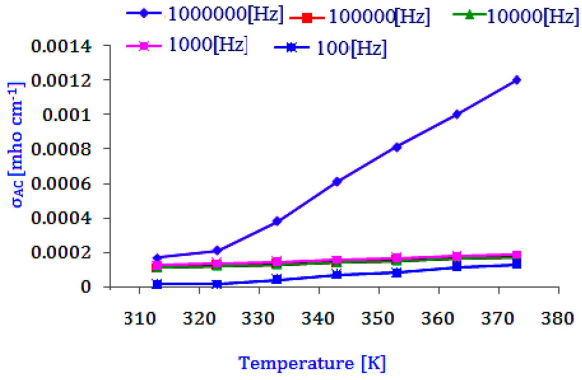


Fig. 5. The AC electrical conductivities for synthesized AMPF micro-crystal.

micro-crystal had good optical quality with lower defects, and these types of materials play an important role in the fabrication of optoelectronic, photonic, photovoltaic and NLO device applications [11].

3.3. AC conductivity, activation energy for μ -AMPF

Electrical conductivity in the synthesized samples is primarily due to the electron hopping between ions, which are uniformly spread over crystallographically identical lattice sites. Pollak [11] showed that conductivity is an increasing frequency function in the case of hopping conductivity and a decreasing frequency function in the case of band conduction. Generally, the overall conductivity is the sum of the hopping and the band sections [12, 13]. In order to compare the conduction mechanism of AC conductivity with the action $n(T)$, different theoretical models have been proposed. As n increases with temperature, the prevailing mechanism is a small polaron, while large polaron overlap is characterised by a minimum accompanied by a rise in n with further increase in temperature. Quantum mechanical tunnelling is predicted in the case when n is temperature-independent, and correlated barrier hopping is normally associated with n decreasing with temperature [14]. The predominance of the small polaron hopping behaviour mechanism is obviously to be noted. In the current study, AC conductivity is measured based on dielectric measurements. It shows that real conductivity increases as the frequency increases — this is the natural conduct of semiconducting materials. The rise in σ_{AC} with applied frequency can be explained on the basis that the pumping force of the frequency applied contributes to the transition between different located states of charge carriers, as well as to the release from different trapping centres of trapped charges. In the conduction phase, these charge carriers participate simultaneously with electrons formed from valence exchange between various metal ions [15]. The variation in

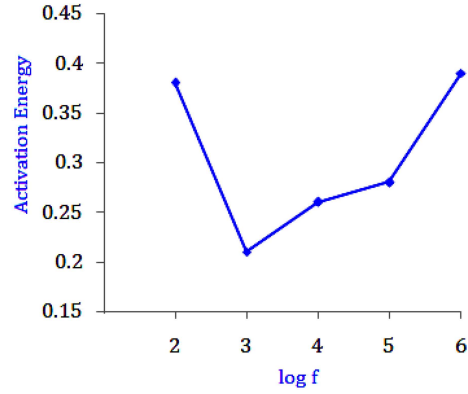


Fig. 6. Frequency dependence of AC activation energy for AMPF micro-crystal.

electrical conductivity with frequency for the synthesised AMPF micro-crystal at various temperatures is shown in Fig. 5. It is noted that the conductivity increases steadily at low frequencies and increases strongly at high frequencies. However, as the frequency increases, conductivity becomes more and more dependent on frequency. The very fundamental reality of AC conductivity in disturbed solids is that it is an increase in frequency. It is possible to distinguish various characteristic frequency regions in the hopping model [16, 17]. At low frequencies, where the conductivity is constant, the transport takes place along infinite paths. In the case of frequency regions where conductivity increases strongly with frequency, the transport is dominated by the contribution of hopping infinite clusters.

The electrical conduction mechanism can be clarified in relation to the electron hopping model in which the conduction mechanism is due to electron hopping between lattice sites. As a consequence, a rise in frequency increases the hopping frequency of charge carriers, which results in an increase in the conduction phase, thus increasing the conductivity. The main objective of the present work is to bring the temperature dependence of conductivity into the picture. The temperature dependence of AC conductivity of synthesized AMPF micro-crystals at various frequencies is depicted in Fig. 5. It is seen that the AC conductivity of the synthesized sample increases with temperature for all defined frequencies. This observation is in good agreement with the well-known conductivity behaviour of semiconductors [18]. Thus, once again, we can conclude from this study that the micro-crystalline AMPF sample exhibits semiconductor behaviour. Interestingly, in Fig. 5, it can be seen that the rate of increase of conductivity is larger at low temperatures compared to that at higher temperatures. Of late, conductivity at lower temperatures is due to thermally induced electrons [19]. Further addition of thermal energy above a certain temperature will resolve the electric field effect in the AMPF micro-crystal, which leads to a reduction of internal

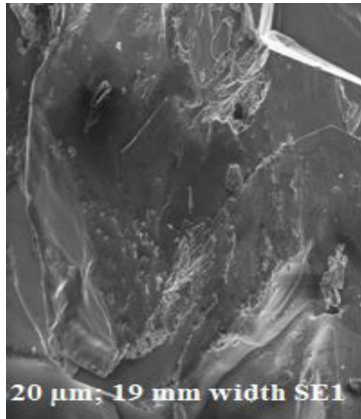


Fig. 7. SEM of 20 μm -AMPF with 50 \times magnified image.

viscosity and hence an increase in the degree of freedom for dipoles (i.e., the entropy of material). Finally, this results in slowing down the growth of AC conductivity at a higher temperature, and thus makes it steady. From the obtained dielectric values of the AMPF sample, AC conductivity is determined.

The mechanism of the electrical conductivity is regulated by the thermal activation process [20]. The slope value is determined from a plot between σ_{AC} vs $1000/T$. The estimated activation energies are observed to decrease with increasing frequency (Fig. 6), which is due to charge carriers hopping between the localised states [21–29]. Normally AC conductivity is opposed to the activation energy. The small fraction of the activation energy derived from AC conductivity calculation is an additional advantage in the fabrication of electro-optical devices.

3.4. SEM study of micro-AMPF crystals

The morphological image of AMPF crystal specified in Fig. 7 confirms the better sample size range by means of average value. The micro-samples of 20 μm -AMPF portrayed in Fig. 7 are a variant in scaling of the grown bulk to a micro-level obtained by using the 10 kV power supply with 19 mm widths and 500X magnifications using a ZEISS type of SEM instrument. This result is proof that microscaled AMPF is devoid of any imperfection and have some inner projections and hollow space-like projective structure and zones, and no crack are observed in the specimen. Similar SEM images are referred to in recent works [21–29].

3.5. Absorbance, Tauc's plot and fluorescence (FL) studies of micro-AMPF crystals

Micro-AMPF is analyzed for absorbance spectra (see Fig. 8) and it can be observed that the cut-off value of 260 nm is an increased cut-off value

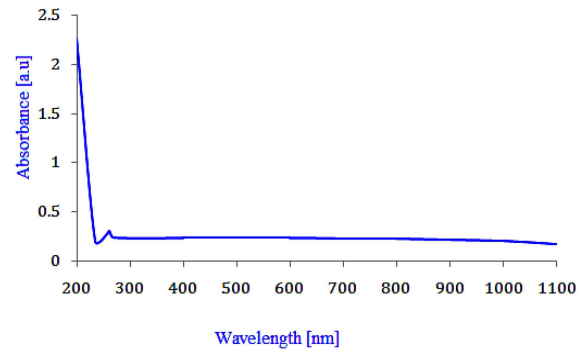


Fig. 8. Absorbance spectrum of AMPF micro-crystal.

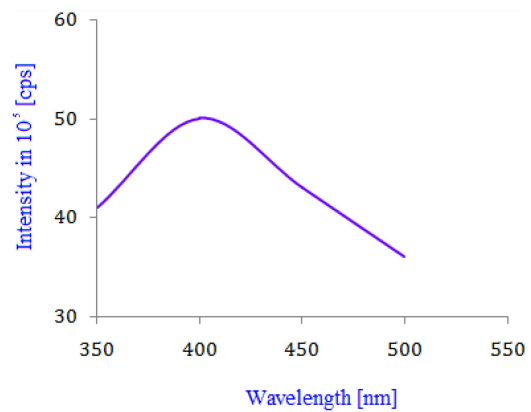


Fig. 9. FL spectrum of AMPF micro-crystal.

than that of bulk-AMPF, thus representing the energy gap of 4.769 eV. From 290 to 1100 nm the absorbance is nearly zero. The results shown in Fig. 8 predominantly confirm the non-linear behaviour for micro-AMPF crystal. Here, the photonic effectiveness for micro-AMPF is exponential by means of the Tauc's plot, which reveals the band gap of 4.77 eV. This is more or less matched with the UV-Visible spectrum, profoundly used in photonics. Regarding the fluorescence (FL) study of micro-AMPF (see Fig. 9), the FL cut-off value of 390 nm (band gap of 3.1794 eV) is slightly reduced than that of bulk AMPF. However, it maintains a correspondence to the violet FL emission for changing range and LED uses [21–29].

3.6. AMPF photoconductive behavior, electronic and phase matching impact in AMPF crystals as well as α -glucosidase based anti-diabetic activity

Representative behavior of photoconductivity is observed for micro-AMPF based on the dark current as well as photocurrent profile in Fig. 10. The dark current goes ahead the photocurrent, thus specifying the photoconductivity nature of micro-AMPF for the functionality of the electronic device. The NLO is of 55 mV input. The phase-matched output of 121 mV is pronounced for particles smaller

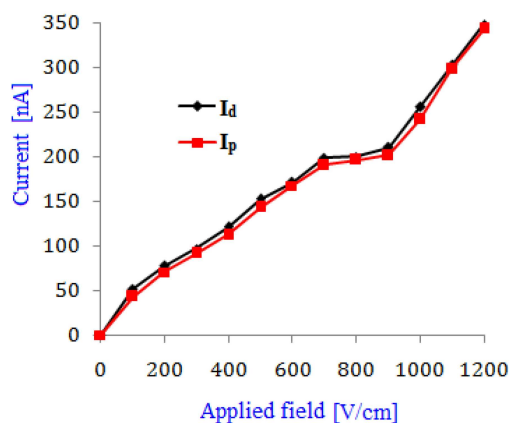


Fig. 10. Photo conducting analysis of μ -AMPF crystal.

than 50 μm and additionally pronounced for other μm of versatile scales, as can be confirmed by reference to earlier works [21–29]. The nano-influx of AMPF is 4.9989 micrometers and is a sign of filter influxing at nano level as higher in value over bulk AMPF and micro-scale AMPF. The LM-317 controlling the voltage represents 16.1 V for micro-AMPF encrusted one with 20 Ω and 236 Ω as values of counter parting resistors which is a good and optimal assessment.

To demonstrate the α -glucosidase-based anti-diabetic activity of AMPF, the half maximal inhibitory concentration IC_{50} is used as a good tool. For micro and nano AMPF, IC_{50} is equal to 61.08 and 58.12, respectively. In the in-vitro methodology, nano AMPF is preferred as an anti-diabetic better scoping agent; the efficacy is due to the presence of chemical functionalities such as fumarate and pyridine in the AMPF crystal cluster.

4. Conclusions

The μ -AMPF crystals are properly obtained by the milled impact of as-grown macro-AMPF by slow evaporation method; the bulk ones are characterized by the parameters equal to 5.0234, 20.0146, 10.8852 — all in units of \AA ; and $\beta = 95.767^\circ$. The micro-crystals are confirmed by a morphological pattern by SEM studies. The dielectric of micro-AMPF crystals are evaluated by the effect on μ -dielectric constant and loss factors, and properly recognized the appropriateness as a semi-conducting material and in the electro-optical device fabrication. Absorbance, photonic, and FL studies pertaining to μ -AMPF allow us to determine (i) cut-off value of 260 nm and 290–1100 nm range representing near-zero absorbance and projected for NLO material applications; (ii) band gap value of 4.77 eV obtained by Tauc's plot; and (iv) value 390 nm obtained with the violet fluorescence emission. The negative type of photoconductivity is

observed for μ -AMPF, and the non-linearity seen in the absorbance study is the reason for applying a phase matching with 121 mV for a referenced value of 55 mV. The nano-influx for AMPF is 4.9989 μ . The α -glucosidase based anti-diabetic activity of micro- as well nano-AMPF represents IC_{50} as 61.08 and 58.12, respectively, due to the presence of fumarate and pyridine in the AMPF crystal cluster. Thus, the objective is clearly pronounced for light-related micro-photonic, electronic and pharmaceutical applications.

Acknowledgments

The authors thank St. Joseph's College for the studies, IITM for data. All the data are included in this paper and no separate repository or representation of data.

References

- [1] A. Thakur, P. Mathur, M. Singh, *J. Phys. Chem. Solids* **68**, 378 (2007).
- [2] A.G. Lone, R.N. Bhowmik, *AIP Adv.* **5**, 047117 (2015).
- [3] C. Prakash, J.S. Baijal, *J. Less Common Met.* **107**, 51 (1985).
- [4] C.G. Koops, *Phys. Rev.* **83**, 121 (1951).
- [5] E.M. Mohammad, K.A. Malins, P. Kurian, M.R. Anantharaman, *Mater. Res. Bull.* **37**, 753 (2002).
- [6] G. Sathishkumar, C. Venkataraju, R. Murugaraj, K. Sivakumar, *J. Mater. Sci. Mater. Electron.* **23**, 243 (2012).
- [7] G. Uzma, *Chin. Phys. B* **23**, 057502 (2014).
- [8] H.G. Zhang, J. Zhou, Y. Wang, L.T. Li, Z.X. Yue, *Mater. Lett.* **55**, 351 (2002).
- [9] J. Parashar, V.K. Saxena, Jyoti, D. Bhatnagar, K.B. Sharma, *J. Magn. Magn. Mater.* **394**, 105 (2015).
- [10] L.L. Hench, J.K. West, *Principles of Electronic Ceramics*, Wiley, New York 1990.
- [11] M. Pollak, in: *Proc. of the Int. Conf. on Physics of Semiconductors*, Exeter 1962, p. 86.
- [12] N.Y. Maharani, A. Cyrac Peter, S. Gopinath, S. Tamilselvan, M. Vimalan, I. VethaPotheher, *J. Mater. Sci. Mater. Electron.* **27**, 5006 (2016).
- [13] A.M. Abo El Ata, M.K. El Nimra, S.M. Attia, D. El Kony, A.H. Al-Hammadi, *J. Magn. Magn. Mater.* **297**, 33 (2006).
- [14] H.M. Zaki, *J. Alloys Compd.* **439**, 1 (2007).
- [15] E. Ateia, M.A. Ahmed, S.I. El-Dek, *J. Mater. Lett.* **57**, 4256 (2003).
- [16] H. Bottger, V.V. Bryksin, *Hopping Conduction in Solids*, Berlin 1985.

- [17] H.M. Zaki, *Physica B* **363**, 232 (2005).
- [18] R.P. Mahajan, K.K. Patankar, M.B. Kothale, S.A. Patil, *Conduct. Bull. Mater. Sci.* **23**, 273 (2000).
- [19] J.R. Macdonald, *Impedance Spectroscopy: Emphasizing Solid State Material and Systems*, Chs. 2 and 4, Wiley, New York 1987.
- [20] S. Abed, H. Bougharraf, K. Bouchouit, Z. Sofiani, B. Derkowska-Zielinska, M.S. Aida, B. Sahraoui, *Superlattice Microstruct.* **85**, 370 (2015).
- [21] R. Ertuğrul, A. Tataroglu, *Chin. Phys. Lett.* **7**, 077 (2012).
- [22] R. Senthilkumar, K. SenthilKannan, S. Udhayakumar, S.T. AadithyaNarayanan, *Mater. Today Proc.* **33**, 4167 (2020).
- [23] K. SenthilKannan, B. Kaleemullah Khan, H. Abdul JaffarAli, V. Kumar Ponnusamy, N. Murugaraj Govindan, *Mater. Today Proc.* **33**, 2779 (2020).
- [24] K. SenthilKannan, R. Krishnaveni, D. Anbuvel, V.M. Porselvi, H. Abdul Jaffar Ali, *Mater. Today Proc.* **33**, 2776 (2020).
- [25] R. Sathishkumar, K. SenthilKannan, C.J. Magesh, K. Venkatapathy, M. Vimalan, D. Sankar, S. Tamilselvan, *Optik*, (2021).
- [26] K. Suganya, J. Maalmarugan, R. Manikandan, T.S. Nagaraj, R.P. Patel, K. Tamilarasi, M. Vimalan, K. SenthilKannan, *J. Mater. Sci. Mater. Electron.* **33**, 19320 (2022).
- [27] V. Sathiya, K. Suganya, K. SenthilKannan, R. Manikandan, *J. Mater. Sci. Mater. Electron.* **33**, 19514 (2022).
- [28] X.V. Winston, D. Sankar, K. SenthilKannan, M. Vimalan, T.R. Kumar, *J. Mater. Sci. Mater. Electron.* **33**, 20616 (2022).
- [29] K. SenthilKannan, *Res. Chem.* **4**, 100424 (2022).